

**ROLE AND CORRELATION OF SYNTHESIS, SIZE AND MORPHOLOGY  
TO THE MAGNETIC PROPERTIES OF COBALT AND COBALT/GOLD  
BIMETALLIC HIERARCHICAL NANOSTRUCTURES**

**by**

**KHE CHENG SEONG**

**Thesis submitted in fulfillment of the requirements  
for the degree of  
Doctor of Philosophy**

**May 2013**

## ACKNOWLEDGEMENTS

Many people whoever contributed to this work and helped me slowly came into my mind one by one. I truly appreciate and cherish what all of you have done for me, even though my gratitude is beyond words. First of all, I would like to express my sincere thanks to my main supervisor Prof. Dr. Azizan b. Aziz for his careful, kindly and constructive guidance during the entire period of my Ph.D study. I also would like to thank my co-supervisor Assoc. Prof. Dr. Zainovia Lockman for the guide, help and trust all the times.

I would like to thank Prof. Dr. Hanafi b. Ismail, Dean of the School of Materials and Mineral Resources Engineering USM, Prof. Dr. Zainal Arifin b. Ahmad and Assoc. Prof. Dr. Syed Fuad b. Saiyid Hashim, Deputy Deans of the School of Materials and Mineral Resources Engineering, for their continuous motivation, cultivated briefing on the postgraduate project and showing helpful in postgraduate affairs throughout my studies. I would like to extend my sincere appreciation to all lecturers in this school for giving me support and guidance.

I also would like to thank all the laboratory technicians and administrative staff of the School of Materials and Mineral Resources Engineering for their kind and patient helps for my work and life. Here, a special appreciation goes to Madam Fong, Mr. Zulkurnain from School of Materials and Mineral Resources Engineering and Madam Faizah of the School of Biological Science, their assistance will always being remembered. Special thanks also go to Mr. Ho from CREST for the assistance in HRTEM.

My sincere thanks also goes to my friends: Wei Wen, Pi Lin, Pek Ling, Steven, Thiem Leng, Yeng Hok, Gaik Tin, Keat Teong, Nisa, Roselina, Junidah and others whom I always remember. Thank you for your friendship and company.

For my parents and siblings, words are not enough to express my gratitude for you. Without your selfless love and endless support, I can not be me today. Thank you for always being there.

Finally, I am very much indebted to the Universiti Sains Malaysia for providing me the financial support under Research University Postgraduate Research Grant Scheme (RU-PRGS) (Project: A/C No: 8042001). I also would like to thank Universiti Sains Malaysia for giving me the USM Fellowship scholarship throughout the PhD study.

Khe Cheng Seong

May 2013

## TABLE OF CONTENTS

	<b>Page</b>
ACKNOWLEDGEMENTS .....	ii
TABLE OF CONTENTS .....	iv
LIST OF TABLES .....	ix
LIST OF FIGURES .....	xii
LIST OF ABBREVIATIONS .....	xxii
LIST OF SYMBOLS .....	xxiv
ABSTRAK .....	xxvi
ABSTRACT .....	xxviii
CHAPTER 1 - INTRODUCTION	
1.1 Nanomaterials .....	1
1.2 Hierarchical nanostructures.....	1
1.3 Background study and problem statement .....	2
1.4 Objective of work.....	7
1.5 Scope of work.....	7
CHAPTER 2 - LITERATURE REVIEW	
2.1 Introduction to nanomaterials .....	8
2.2 Size and surfaces in nanomaterials .....	9
2.3 Hierarchical nanostructures .....	13
2.4 Synthesis approaches of various type of nanomaterials /nanostructures	15
2.4.1 Hydrothermal or solvothermal process .....	16
2.4.2 Polyol process .....	22

2.4.3	Galvanic replacement reaction .....	28
2.5	Magnetic materials .....	31
2.5.1	Magnetic anisotropy .....	37
2.5.2	Law of approach to saturation .....	40
2.6	Organisation of Magnetic Nanomaterials With Hierarchical Structure: effect of different synthetic conditions .....	43
2.6.1	Effect of starting precursor .....	44
2.6.2	Effect of reaction time .....	45
2.6.3	Effect of reaction temperature .....	46
2.6.4	Effect of NaOH .....	47
2.6.5	Effect of reducing agent .....	47
2.6.6	Effect of surfactant .....	49
2.7	Optical properties .....	52
2.7.1	Optical properties of cobalt and bimetallic cobalt/gold particles.....	56
2.8	Potential applications of hierarchical and bimetallic magnetic materials.....	57
2.8.1	Microwave absorber .....	57
2.8.2	Catalyst .....	57
2.8.3	Optical imaging .....	58
2.8.4	Other potential applications .....	59

### CHAPTER 3 - MATERIALS AND METHODS

3.1	Raw materials and the preparation of reactant solutions.....	60
3.2	Synthesis of cobalt nanostructures.....	60
3.2.1	Effect of reaction temperature .....	63

3.2.2	Effect of reaction time .....	63
3.2.3	Effect of concentration NaOH .....	64
3.2.4	Effect of reducing agents .....	64
3.2.5	Effect of concentration of cobalt precursor .....	65
3.2.6	Effect of Surfactants .....	66
3.3	Synthesis of Cobalt/Gold Bimetallic particles .....	68
3.4	Centrifugation and washing process .....	70
3.5	Sample characterisation .....	70
3.5.1	X-Ray Diffraction (XRD) .....	71
3.5.2	Scanning electron microscopy (SEM) .....	71
3.5.3	Transmission electron microscopy (TEM) .....	72
3.5.4	Thermogravimetric analysis (TGA) .....	73
3.5.5	Ultra-violet Visible spectrophotometer (UV- Vis) .....	73
3.5.6	Fourier Transform Infrared Spectroscopy (FTIR) .....	73
3.5.7	Vibrating sample magnetometer (VSM) .....	74
3.5.8	Atomic absorption spectrometer (AAS) .....	74
3.5.9	Zeta potential analysis .....	75

#### CHAPTER 4 - RESULTS AND DISCUSSION

4.1	Introduction .....	76
4.2	Synthesis of cobalt hierarchical nanostructures .....	76
4.2.1	Effect of reaction temperature .....	76
4.2.2	Effect of reaction time .....	84
4.2.3	Effect of sodium hydroxide (NaOH) .....	87
4.2.4	Effect of reducing agent .....	98
4.2.4.1	Effect of Hydrazine .....	99

4.2.4.2	Effect of Sodium Borohydride (NaBH <sub>4</sub> ) .....	109
4.2.5	Effect of cobalt precursor (Cobalt chloride hexahydrate) .....	118
4.2.6	Effect of surfactant .....	125
4.2.6.1	Effect of non-ionic surfactant: Polyvinylpyrrolidone K30 (PVP K30) .....	125
4.2.6.2	Effect of Cationic Surfactant: Cetyltrimethyl ammonium bromide (CTAB) .....	137
4.2.6.3	Effect of anionic surfactant: Sodium Dodecyl Sulfate (SDS) .....	147
4.3	Magnetic Properties of hierarchical cobalt particles with different morphologies at room temperature .....	156
4.3.1	Spherical hierarchical particles .....	157
4.3.2	Hierarchical nanostructures with different morphologies (without surfactant) .....	161
4.3.3	Sample with random aggregates (Effect of sodium Borohydride) .....	165
4.3.4	Hierarchical nanostructures with different morphologies (with surfactant) .....	168
4.4	Synthesis of cobalt/gold bimetallic hierarchical nanostructures .....	173
4.4.1	Effect of concentration of H <sub>2</sub> AuCl <sub>4</sub> .....	173
4.4.2	Effect of reaction temperature .....	185
4.4.3	Effect of NaOH .....	191
4.5	Magnetic properties of cobalt/gold bimetallic nanostructures .....	198
4.5.1	Magnetic properties of cobalt/gold samples synthesised with different H <sub>2</sub> AuCl <sub>4</sub> concentration .....	199
4.5.2	Magnetic properties of cobalt/gold samples synthesised with different reaction temperatures.....	203
4.5.3	Magnetic properties of cobalt/gold samples synthesised with different NaOH concentrations.....	207

## CHAPTER 5 - CONCLUSION AND RECOMMANDATIONS

5.1	Conclusions .....	212
5.2	Recommendations for future works .....	214
	REFERENCES .....	216
APPENDICES		
APPENDIX A	Calculation of saturation magnetisation of the bimetallic particles .....	239
APPENDIX B	Indexing the Selected Area Electron Diffraction (SAED) ...	240
APPENDIX C	Zeta potential of cobalt particles .....	245
APPENDIX D	UV-Vis spectroscopy of mixture H <sub>Au</sub> Cl <sub>4</sub> in Ethylene glycol with NaOH .....	247
	LIST OF PUBLICATIONS .....	249

## LIST OF TABLES

		<b>Page</b>
Table 1.1	Cobalt hierarchical particles synthesised via polyol process in the past.	5
Table 1.2	Co/Au hierarchical bimetallic particles produced from galvanic replacement reaction in the past.	6
Table 2.1	Different anisotropic nanomaterials group with different dimensionality (Rotello, 2004a).	9
Table 2.2	Various materials with hierarchical structure synthesised via hydro/solvothermal in the recent years.	22
Table 2.3	Standard electrode potentials of different materials.	29
Table 2.4	The arrangement of magnetic moments for four principle classes of magnetism.	33
Table 2.5	Anisotropy constants, K, for various materials.	38
Table 2.6	Magnetic properties (at 300K) of cobalt hierarchical particles with different sizes and morphologies	51
Table 3.1	Chemicals used in the synthesis	61
Table 3.2	Synthesis parameters for the study of different reaction temperatures.	63
Table 3.3	Synthesis parameters for the study of different reaction times	64
Table 3.4	Synthesis parameters for the study of effect of NaOH concentration.	64
Table 3.5	Synthesis parameters for the study of effect of reducing agent (Hydrazine Hydrate)	65
Table 3.6	Synthesis parameters for the study of effect of reducing agent (sodium borohydride)	65
Table 3.7	Synthesis parameters for the study of effect of cobalt precursor	66
Table 3.8	Synthesis parameters for study of different concentrations of non-ionic surfactant, polyvinylpyrrolidone K30 (PVPK30)	67

Table 3.9	Synthesis parameters for study of different concentrations of cationic surfactant, Cetyl trimethyl amonium bromide (CTAB)	67
Table 3.10	Synthesis parameters for study of different concentrations of anionic surfactant, Sodium Dodecyl Sulfate (SDS)	67
Table 3.11	Experimental details in effect of gold salt concentration study	69
Table 3.12	Experimental details in effect of NaOH study	70
Table 3.13	Experimental details in effect of reaction temperature study	70
Table 4.1	Crystallite size of cobalt particles obtained with different concentrations of NaOH	88
Table 4.2	Comparison of the element weight percent when the NaOH concentration increased	94
Table 4.3	Information extracted from TG curves	96
Table 4.4	pH of the solution with different concentrations of cobalt chloride	124
Table 4.5	Parameters obtained from the M-H curves for different samples with spherical shape	160
Table 4.6	Parameters obtained from the M-H curves for different samples with different morphologies	164
Table 4.7	Parameters obtained from the M-H curves for different samples with different NaBH <sub>4</sub> concentrations	167
Table 4.8	Parameters obtained from the M-H curves for different samples with assistance of different surfactants	171
Table 4.9	Parameters obtained from the M-H curves for the bimetallic samples synthesised with different HAuCl <sub>4</sub> concentrations.	201
Table 4.10	Percentage of the cobalt contents in the bimetallic samples and the Ms values after conversion.	202
Table 4.11	Parameters obtained from the M-H curves for different bimetallic samples synthesised with different reaction temperatures	205
Table 4.12	Percentage of the cobalt contents in the bimetallic samples and the Ms values after conversion.	206

Table 4.13	Parameters obtained from the M-H curves for different bimetallic samples synthesised with different NaOH concentrations	209
Table 4.14	Percentage of the cobalt contents in the bimetallic samples and the Ms values after conversion.	210

## LIST OF FIGURE

	<b>Page</b>	
Figure 2.1	Nanomaterials lie at the intersection of materials science, physics, chemistry and biology or medicine (Vollath, 2008)	8
Figure 2.2	The percentage of surface atoms changes with the palladium cluster diameter (Nutzenadel et al., 2000)	10
Figure 2.3	Two particles with face-to-face contact and coherent interfacial matching (Wang and Feng, 2003)	12
Figure 2.4	Nomenclature of hierarchical structures according to the dimensions of the nano-building blocks (the former number) and of the consequent hierarchical structures (the latter number) (Lee, 2009)	14
Figure 2.5	Illustration showing the top down, intermediate and bottom up approaches to make bulk nanostructured solids (Ashby et al., 2009)	16
Figure 2.6	SEM images of nickel hierarchical nanostructures with (a) urchin like and (b) sisal like morphologies	18
Figure 2.7	(a,b) SEM and (c,d) TEM images of the Co nanoflowers (liu et al. 2009a)	19
Figure 2.8	(a) Typical SEM image of PbTe hierarchical nanostructures. Inset: unit cell of PbTe. (b) Magnified image of a hopper cubic crystal. (c) Magnified image of a flower-like crystal. (d) EDX spectrum of PbTe superstructures (Zhu et. al., 2009)	20
Figure 2.9	SEM pictures of ZnO NW nanoforest: (a) tilted view, (b) crosssection view, (c) TEM picture and selected area electron diffraction pattern of a ZnO NW (Ko et al., 2011)	21
Figure 2.10	(a) SEM image of the as-synthesised Ni microspheres chain network (b) magnified image of single hollow microsphere with hierarchical structure (Wang et at., 2008b)	24
Figure 2.11	(a) TEM image of the nanoflowers, (b) a high-magnification TEM of a single nanoflower with hierarchical nanostructures (Xu et al., 2008)	25

Figure 2.12	SEM images of ZnO nanoparticles prepared by (a) heating the precursor solution and (b) water injection into hot precursor solution (Lee et al., 2008)	26
Figure 2.13	Scanning electron microscopy (SEM) images of the morphologies of LiFePO <sub>4</sub> obtained by polyol process (Singh and Willert-Porada, 2011)	27
Figure 2.14	TEM image (a) and HRTEM image (b) of an individual star-shaped PbS multipods with six arms. HRTEM image and SAED pattern (inset of a) are both obtained from the area marked with square in the arm. (c) SEM image and (d, e) elemental analysis of star-shaped PbS (Quan et al., 2008).	28
Figure 2.15	(a) Low and (b) high magnification of SEM images of the hierarchical Co-Au micro wires with nanoflakes (Min et al., 2011).	31
Figure 2.16	Schematic illustration of the hysteresis loops of ferromagnetic materials. $M_s$ = saturation magnetic moment; $M_r$ = remnant magnetic moment; $H_c$ = coercivity (Sun, 2006).	35
Figure 2.17	Scheme for coercivity as a function of particle size (Hadjipanayis, 1999).	36
Figure 2.18	Schematic illustration of the materials with superparamagnetic behaviour. No coercivity and only saturation magnetic moment is obtained.	36
Figure 2.19	Single domain size, $D_{crit}$ and superparamagnetic limit at room temperature, $D_{sp}$ for some common ferromagnetic materials (Krishnan et al., 2006).	37
Figure 2.20	External field applied along (a) long axis of wire, (b) short axis of wire, where $H_D$ = demagnetizing field, $H_{ext}$ = External field. Demagnetizing field will be lower at the long axis due to the poles far apart.	40
Figure 2.21	SEM images of the cobalt oxide hierarchical particles prepared with different concentrations of cobalt acetate at (a) 6, (b) 40, (c) 93, and (d) 160 mM (Cao et al., 2006)	45
Figure 2.22	SEM images of the samples prepared at different temperatures: (a) 180 °C, (b) 160 °C, (c) 140 °C, (d) 120 °C (Zhang et al., 2008b).	47

Figure 2.23	(a) SEM and (b) TEM images of hierarchical magnetite microspheres. Rough surface (from SEM) and the contrast from TEM confirmed the particles are hierarchical structures (Zhao et al., 2010).	50
Figure 2.24	Schematic of plasmon oscillation for a sphere, showing the displacement of the conduction electron charge cloud relative to the nuclei (Kelly et al., 2003).	52
Figure 2.25	UV-visible NIR spectrum obtained from a dispersion of nanostructures in water, while inset shows the portion of the spectrum enlarged in the range 250-650 nm for clarity (Sharma et al., 2008).	55
Figure 3.1	Flow Chart shows the polyol process in the preparation of cobalt nanostructures.	62
Figure 3.2	Experimental setup for the polyol process in the current study.	62
Figure 3.3	Flow Chart shows the polyol process in preparation of cobalt nanostructures with surfactant.	68
Figure 3.4	Typical experimental procedures for the preparation of Co/Au bimetallic nanostructures.	69
Figure 4.1	XRD patterns of the samples synthesised at lower temperatures (a) 60°C, (b) 70°C (c) 80°C and (d) 100°C (# = cobalt hydroxide; * = unidentified phase)	77
Figure 4.2	UV-Vis spectra of the supernatants of different samples after reaction of 1 hour at different temperatures (T130 = 130°C, T150 = 150°C, T170 = 170°C and T190 = 190°C)	78
Figure 4.3	XRD patterns of the cobalt powder with different reaction temperatures (a) 130°C, (b) 150°C, (c) 170°C and (d) reflux temperature (190°C).	80
Figure 4.4	Cobalt particles with different reaction temperatures (a,b) 130°C, (c,d) 150°C (e,f) 170°C and (g,h) 190°C.	81
Figure 4.5	Average hierarchical particle size of the samples synthesised with different reaction temperatures.	82
Figure 4.6	EDX for cobalt particles prepared from different reaction temperatures (a) 130°C (b) 150°C (c) 170°C and (d) 190°C.	83
Figure 4.7	XRD patterns of the samples synthesised with different	84

	reaction times (a) 90 min (b) 120 min and (c) 150 min.	
Figure 4.8	SEM micrographs (with low and higher magnifications) for the samples with different reaction times (a-b) 90 min (c-d) 120 mi and (e-f) 150 minutes.	85
Figure 4.9	Average particle size for the hierarchical particles with different reaction times.	86
Figure 4.10	Schematic diagram represent Ostwald ripening process that occurred in cobalt nanoparticles when the reaction time increased (modified from Wikipedia 2012).	87
Figure 4.11	XRD patterns of the samples synthesised with different concentrations of NaOH (a) 0.5M (OH 1), (b) 0.75M (OH 2), (c) 2.0M (OH 3) and (d) 3.0M (OH 4).	88
Figure 4.12	SEM micrographs (with low and high magnifications) for the samples synthesised with different concentrations of NaOH, (a-b) sample OH 1, (c-d) sample OH 2, (e-f) sample OH 3 and (g-h) sample OH 4.	91
Figure 4.13	Average particle size of hierarchical microspheres formed with different concentrations of NaOH.	92
Figure 4.14	HRTEM images of the sample OH 4 (a) low magnification, (b) High magnification, (c) selected area electron diffraction (SAED) from the surface of the particles, (d) high resolution image with the lattice fringes are clearly observed.	93
Figure 4.15	EDX spectra of samples with different concentrations of NaOH (a) 0.5M (b) 0.75M, (c)2.0 M and (d) 3.0M.	94
Figure 4.16	TGA of the samples prepared in different NaOH concentrations (OH 1= 0.5M, OH 2 = 0.75M, OH 3 = 2.0 M and OH 4 = 3.0M).	95
Figure 4.17	XRD patterns of the as prepared samples with different molar ratio of $N_2H_4$ to $Co^{2+}$ (a) 2.5 (NH 1), (b) 5.5 (NH 2), (c) 7.5 (NH 3) and (d) 10.0 (NH 4). Inset shows the magnified XRD patterns which clearly show the peak shifted from sample NH1 to NH 4.	100
Figure 4.18	Cobalt samples synthesised with (a-b) 2.5 (c-d) 5.5 (e-f) 7.5 molar ratio of $N_2H_4$ to $Co^{2+}$ .	102
Figure 4.19	(a) SEM image of cobalt particles synthesised with 10.0 molar ratio of $N_2H_4$ to $Co^{2+}$ with raspberry morphology. Inset shows the photograph of raspberry. (b) Magnified SEM image and inset shows TEM image of the raspberry like cobalt particles.	103

Figure 4.20	(a) TEM image of a single particle of NH <sub>4</sub> (b) magnified area from (a) with white circle (c) high resolution image from the magnified area (d) SAED pattern of (b).	104
Figure 4.21	Average particle size of hierarchical microspheres decreasing with the increasing molar ratio of N <sub>2</sub> H <sub>4</sub> to Co <sup>2+</sup> .	105
Figure 4.22	EDX spectra of the cobalt powder obtained from different molar ratio of hydrazine hydrate to cobalt ions (a) 2.5, (b) 5.5, (c) 7.5 and (d) 10.0.	106
Figure 4.23	(a) Thermogravimetric analysis of samples synthesised with different concentration of hydrazine (b) derivative weight change of different samples.	107
Figure 4.24	XRD patterns of the as prepared samples with different molar ratio of BH <sub>4</sub> <sup>-</sup> to Co <sup>2+</sup> (a) 2.5 (NB1), (b) 5.5 (NB 2), (c) 7.5 (NB 3) and (d) 10.0 (NB 4).	110
Figure 4.25	SEM images of samples prepared with different molar ratio of BH <sub>4</sub> <sup>-</sup> to Co <sup>2+</sup> (a) NB1 (b) NB 2 (c) NB 3 and (d) NB 4.	110
Figure 4.26	TEM micrographs of samples prepared with NaBH <sub>4</sub> (a) NB1 (b) NB2 (c) NB3 and (d) NB 4, (e) and (f) representative EELS spectroscopy for the samples show the contain of cobalt and boron.	112
Figure 4.27	EDX of samples prepared with different molar ratio of BH <sub>4</sub> <sup>-</sup> to Co <sup>2+</sup> (a) NB 1 (b) NB 2 (c) NB 3 and (d) NB 4.	113
Figure 4.28	FTIR spectra of the samples prepared with different molar ratio of BH <sub>4</sub> <sup>-</sup> to Co <sup>2+</sup> (a) NB 1 (b) NB 2 (c) NB 3 and (d) NB 4.	114
Figure 4.29	Thermogravimetric analysis of samples prepared with different molar ratio of BH <sub>4</sub> <sup>-</sup> to Co <sup>2+</sup> (a) NB 1 (b) NB 2 (c) NB 3 and (d) NB 4.	116
Figure 4.30	XRD patterns of (a) NB 1 and (b) NB 4 after heat treatment at 900°C.	117
Figure 4.31	FTIR spectra of the samples after thermogravimetric study, (a) NB 1 (b) NB 2 (c) NB 3 and (d) NB 4.	117
Figure 4.32	SEM micrographs for samples prepared with different concentrations of cobalt chloride (a-b) 10 mM (CE 1) (c-d) 15 mM (CE 2) and (e-f) 30 mM (CE 3). Insets in (a) and (e) are the TEM images.	120

Figure 4.33	(a) SEM micrograph for sample CE 4, inset shows the TEM image. (b) Magnified SEM image with small nano-sized particles can be seen on the particle surface.	121
Figure 4.34	Sample CE 4, (a) TEM image (b) magnified image from (a) the area with a white circle (c) high resolution TEM image (d) SAED from the area (b).	122
Figure 4.35	Average particle size of hierarchical samples synthesised with different cobalt concentrations.	123
Figure 4.36	XRD patterns of the samples synthesised with different concentration of $\text{CoCl}_2$ . Sample (a) CE 1 (b) CE 2 (c) CE 3 and (d) CE 4.	123
Figure 4.37	XRD patterns for the as prepared cobalt particles with different PVP contents. Inset shows the (002) peaks slightly shifted to lower $2\theta$ from (a) Purely Co (b) PVP1 (1.5% w/v), (c) PVP2 (2.0% w/v), (d) PVP3 (2.5% w/v) and (e) PVP4 (3.0% w/v).	126
Figure 4.38	SEM images of different samples synthesised with different PVP contents (a) control sample without PVP (b) PVP1 (c) PVP2 (d) PVP3 (e) PVP4 and (f) magnified image of (e).	127
Figure 4.39	(a)-(c) TEM images of PVP 4 from different viewing angles (d) SEM image. (e) Schematic diagram of a pseudo-model of the perfect truncated hexagonal bipyramid, drawn based on the SEM and TEM images from different viewing angles. Scale bar = 200nm.	128
Figure 4.40	Sample PVP 4, (a) TEM image of a single hexagonal shape cobalt particle (b) small sized nanoparticles can be observed with magnified the TEM image from the edge of the hexagonal shape particle marked with white circle (c) EELS proved that the small sized particles are cobalt.	129
Figure 4.41	HRTEM images for the sample PVP 4 (a) Faceted cobalt nanoparticles were observed (b) SAED of the sample from the (a), (c) twin boundaries formed in the faceted nanoparticles (d) hexagonal shape nanoparticle observed.	131
Figure 4.42	EDX spectra for different samples synthesised with various concentrations of PVP, (a) purely Co (b) PVP 1 (c) PVP 2 (d) PVP 3 and (e) PVP 4.	132
Figure 4.43	FTIR spectra for the (a) Pure PVP (b) sample PVP 2 (c) sample PVP 4.	134

Figure 4.44	Chemical structure of Polyvinylpyrrolidone K30, $n$ represents the polymerization number (Yin et al., 2003).	134
Figure 4.45	TGA spectra for PVP incorporated samples (a) PVP2 (b) PVP3 and (c) PVP 4.	135
Figure 4.46	Molecular structure of CTAB (Modaressi et al., 2007).	137
Figure 4.47	TEM images and histograms for the samples prepared with different concentration of CTAB (a-b) 0.5 % (w/v) (CTAB 1) (c-d) 1.0 % (w/v) (CTAB 2) (e-f) 2.0 % (w/v) (CTAB 3) and (g-h) 3.0 % (w/v) (CTAB 4).	139
Figure 4.48	HRTEM images for the sample CTAB 1 (a) low magnification, inset shows the SAED of the sample (b) lattice resolved image (c) particles with Moire fringes.	140
Figure 4.49	(a-b) SEM and STEM images of pure cobalt particles without surfactant CTAB. SEM images of cobalt particles synthesised with CTAB, (c-d) CTAB 1 (e-f) CTAB 2 (g-h) CTAB 3 (i-j) CTAB 4.	142
Figure 4.50	EDX spectroscopy of cobalt particles prepared with CTAB, (a) CTAB 1 (b) CTAB 2 (c) CTAB 3 (d) CTAB 4.	143
Figure 4.51	XRD patterns for the as prepared cobalt powder (a) CTAB 0 (b) CTAB 1 (c) CTAB 2 (d) CTAB 3 (e) CTAB 4.	144
Figure 4.52	Fourier transform infrared (FTIR) spectroscopy of (a) pure CTAB and (b) CTAB 1 and (c) CTAB 3 (d) CTAB 4.	145
Figure 4.53	TGA curves for samples (a) Pure Co (b) CTAB 2 (c) CTAB 3 (d) CTAB 4.	146
Figure 4.54	Molecular structure of the SDS.	147
Figure 4.55	XRD patterns of samples prepared with different SDS contents, (a) 0.5% w/v (SDS 1), (b) 1.0 wt% w/v (SDS 2), (c) 2.0 wt% (SDS 3) and (d) 3.0wt% (SDS 4).	148
Figure 4.56	SEM images and EDX spectroscopy for the samples prepared with SDS, (a-b) SDS 1 (c-d) SDS 2 (e-f) SDS 3 (g-h) SDS4.	149
Figure 4.57	TEM and SEM (inset) for samples SDS 4 with (a) rectangle (b) quasi cubic (c) irregular rectangle or elongated shape (d) EELS with energy loss of 774 eV.	151
Figure 4.58	TEM images for sample SDS 4 (a) cobalt nanoparticles embedded in organic layer and the corresponding FFT	152

pattern shown in inset (b) lattice resolved high resolution image with (F111/H002) fringes which is magnified from the area with white square from (a).

Figure 4.59	FTIR spectra of pure SDS and samples prepared with SDS, (a) SDS 1 (b) SDS 2 (c) SDS 3 and (d) SDS 4.	153
Figure 4.60	Magnetic hysteresis loop of the hierarchical spherical particles (samples NH1, T190, OH4 and T130).	158
Figure 4.61	High field region of magnetic hysteresis curves fitted with theoretical equation of law of approach to saturation.	159
Figure 4.62	Magnetic hysteresis loop of the samples with various morphologies (a) CE 4 (b) NH 4 (c) OH 1 (d) CE 3.	162
Figure 4.63	Magnetisation curves at high field region fitted with law of approach to saturation.	163
Figure 4.64	Hysteresis loops of samples prepared with different molar ratio of $\text{BH}_4^-$ to $\text{Co}^{2+}$ , (a) NB 1 (b) NB 2 (c) NB 3 and (d) NB 4. (i) Hysteresis loop at high field, (ii) hysteresis loop at low field.	166
Figure 4.65	(a) Magnetisation curves of different samples at high field fitted with law of approach to saturation (b) sample NB 4 solely with lower scale.	167
Figure 4.66	Magnetic hysteresis loops of the samples with various morphologies prepared with the assistant of surfactants, (a) PVP 4 (b) CTAB 4 (c) SDS 4.	170
Figure 4.67	Magnetisation curves at high field region fitted with law of approach to saturation for different samples prepared with surfactants.	170
Figure 4.68	XRD patterns of pure cobalt and cobalt/gold samples prepared with different amount of $\text{HAuCl}_4$ (5mM), (a) pure cobalt, (b) 4ml (CoAuG1), (c) 5ml (CoAuG2) and (d) 6 ml (CoAuG3).	174
Figure 4.69	(a) SEM, (b) TEM micrographs and (c) EDX spectrum for the pure spherical cobalt particles.	176
Figure 4.70	(a) SEM, (b) TEM micrographs and (c) EDX spectrum of the sample CoAuG1 after replacement reaction with addition of 4 ml $\text{HAuCl}_4$ .	177
Figure 4.71	(a) SEM, (b) TEM micrographs and (c) EDX spectrum of the sample CoAuG2 after replacement reaction with addition	179

	of 5 ml $\text{HAuCl}_4$ . Contrast between the edge and the centre of the particle can be seen in the TEM micrograph.	
Figure 4.72	(a) TEM for the sample with hollow structure, and ESI for the same sample (b) blue colour for element cobalt and (c) green colour for element gold (d) sketch of cross-sectional view for the bimetallic hollow particles formed.	171
Figure 4.73	(a) SEM and (b) TEM micrographs for sample CoAuG3 after replacement reaction with addition of 6 ml $\text{HAuCl}_4$ . Broken microspheres can be clearly noticed and pointed with an arrow. The area with square 1 was magnified and shows in (c) and (e). (d) EDX spectrum of the area marked with square in (a). The SAED conducted on the area labeled with 2 was shown in (f) and the lattice resolved image for area 2 was shown in (g).	181
Figure 4.74	TGA curves for (a) cobalt particles (b) CoAuG1, (c) CoAuG2 and (d) CoAuG3.	183
Figure 4.75	UV-Vis spectroscopy for (a) cobalt particles (b) CoAuG1, (c) CoAuG2 and (d) CoAuG3.	185
Figure 4.76	XRD patterns of the cobalt/gold samples synthesised with different temperatures (a) (b) $50^\circ\text{C}$ (c) $80^\circ\text{C}$ (d) $100^\circ\text{C}$ and (e) $120^\circ\text{C}$ .	186
Figure 4.77	Cobalt/gold bimetallic particles obtained from galvanic replacement at $50^\circ\text{C}$ (a) low magnification (b) high magnification (c) EDX spectrum and (d) TEM image (e) SAED (f) high resolution TEM image.	187
Figure 4.78	(a,c,e) SEM images of cobalt/gold bimetallic particles (CoAu T80, T100 and T120 respectively) obtained from galvanic replacement at different temperatures. (b,d,f) Corresponding EDX spectra of the samples CoAuT80, CoAuT100 and CoAuT120.	189
Figure 4.79	UV-vis spectra of different samples synthesised with different reaction temperatures (a) $50^\circ\text{C}$ (b) $80^\circ\text{C}$ (c) $100^\circ\text{C}$ (d) $120^\circ\text{C}$ .	190
Figure 4.80	XRD patterns of the cobalt/gold samples prepared with different amounts of NaOH (1M), (a) 0.10 ml (CoAuN1), (b) 0.20 ml (CoAuN2), (c) 0.25 ml (CoAuN3) and (d) 0.30 ml (CoAuN4).	191
Figure 4.81	Sample CoAuN1 (a) SEM (b) magnified image form (a) with marked with square, (c) EDX spectrum (d) TEM image of a broken sphere.	192

Figure 4.82	Sample CoAuN2 (a) SEM (b) magnified of a hollow sphere with spiky surface (c) EDX spectrum (d) TEM image of spiky hollow sphere (contrast can be seen at lower part).	193
Figure 4.83	Sample CoAuN3 (a) SEM (b) magnified SEM image (c) EDX spectrum (d) TEM image of corroded cobalt sphere.	194
Figure 4.84	Sample CoAuN4, SEM images of (a) gold rich area and (b) cobalt rich area with (c-d) are the EDX spectra for the image (a) and (b) respectively.	195
Figure 4.85	Sample CoAuN4, (a)TEM micrographs (b)Magnified image of (a), (c) High resolution TEM of the area with circle in (b), (d) lattice resolved micrograph from (a), (e) SAED of the area in (d).	197
Figure 4.86	UV-vis spectra of the samples prepared with different concentrations of NaOH, (a) CoAuN1 (b) CoAuN2 (c) CoAuN3 and (d) CoAuN4.	198
Figure 4.87	Magnetic hysteresis loops of samples at (i) high field (ii) low field. (a) Pure cobalt particles, (b) CoAuG1, (c) CoAuG2 and (d) CoAuG3.	199
Figure 4.88	Magnetic curves fitted at high field region for the samples (a) pure Co (b) CoAuG1 (c) CoAuG2 (d) CoAuG3. Solid line represented the fitting from the LAS theoretical equation.	201
Figure 4.89	Magnetic hysteresis loops of different samples synthesised from different reaction temperatures. (a) pure Co (b) 50°C (c) 80°C (d) 100°C and (e) 120°C (i) low field and (ii) high field.	204
Figure 4.90	(i)(a) Sample CoAuT50 and (b) CoAuT80 shows open loops, (ii)(c) CoAuT100 and (d) CoAuT120 fitted with LAS equation.	205
Figure 4.91	Magnetic hysteresis loops of different samples synthesised from different NaOH concentration with (i) high field and (ii) low field; (a) pure Co (b) CoAuN1 (c) CoAuN2 (d) CoAuN3 (e) CoAuN4.	208
Figure 4.92	M-H curves fitted with LAS at high field region for different samples synthesised with different NaOH concentrations, (a) CoAuN1, (b) CoAuN2, (c) CoAuN3, (d) CoAuN4. Solid line represented the fitting from the LAS theoretical equation.	209

## LIST OF ABBREVIATIONS

AAS	Atomic absorption spectroscopy
atm	Atmosphere
CTAB	Cetyl trimethylammonium Bromide
EG	Ethylene glycol
EDX	Energy dispersive X-ray analysis
EELS	Electron energy loss spectroscopy
ESI	Electron spectroscopy imaging
FCC	Face centre cubic
FFT	Fast fourier transform
FTIR	Fourier transform infrared
FWHM	Full width half maximum
HCP	Hexagonal closed packed
HRTEM	High resolution transmission electron microscopy
ICDD	International centre for diffraction data
LAS	Law of approach to saturation
NaOH	Sodium hydroxide
NIR	Near infrared
PVP	Polyvinylpyrrolidone
RPM	Revolutions per minute
SAED	Selected area electron diffraction
SDS	Sodium dodecyl sulphate

SEM	Scanning electron microscopy
SPR	Surface plasmon resonance
TEM	Transmission electron microscopy
TGA	Thermogravimetric analysis
UV-Vis	Ultra violet – visible
VSM	Vibrating sample magnetometer
XRD	X-ray diffraction

## LIST OF SYMBOLS

$\chi$	Magnetic susceptibility
$\theta$	Diffraction angle
$^{\circ}$	Degree
B	Full width at half maximum of a diffraction peak
E	Magnetic anisotropy energy
K	Magnetic anisotropy constant
At %	Atomic percent
Wt %	Weight percent
R	Ratio
$\lambda$	X-ray wavelength
D	Crystallite size
V	Particle volume
$\epsilon_m$	Dielectric function
$\omega$	Angular frequency
c	Speed of light
$K_{\text{eff}}$	Effective anisotropy constant
a	Constant in Law of approach to saturation
b	Constant in Law of approach to saturation
$\chi_p$	Constant in Law of approach to saturation
H	Magnetic field
Hc	Coercivity

M	Magnetisation
M <sub>s</sub>	Saturation magnetisation
D <sub>sp</sub>	Single domain size
D <sub>crit</sub>	Superparamagnetic limit

# **PERANAN DAN HUBUNGAN SINTESIS, SAIZ DAN MORFOLOGI TERHADAP SIFAT MAGNET NANOSTRUKTUR HIERARKI KOBALT DAN KOBALT/EMAS DWILOGAM**

## **ABSTRAK**

Kobalt adalah bahan feromagnet dan partikel kobalt-emas dwilogam dijangka mempunyai modulasi sifat magnet. Selain itu, nanostruktur emas juga merupakan bahan plasmonik yang baik. Walau bagaimanapun, kobalt mudah mengalami pengoksidaan dalam persekitaran berair. Lapisan yang mengalami pengoksidaan boleh merosakkan sifat-sifat magnetnya. Oleh itu, untuk mengelakkan pengoksidaan kobalt, kerja ini menumpukan kepada sintesis partikel kobalt hierarki dan partikel kobalt-emas dwilogam hierarki dengan menggunakan kombinasi kaedah polyol dan tindak balas penggantian galvanik. Keadaan sintesis yang berlainan telah digunakan untuk menyiasat kesannya terhadap morfologi partikel kobalt hierarki yang dihasilkan. Parameter yang dikaji termasuk masa tindak balas, natrium hidroksida, kepekatan garam kobalt, suhu tindakbalas, ejen penurunan dan surfaktan. Pelbagai morfologi telah berjaya disediakan seperti mikrosfera hierarki, bentuk polyhedra hierarki, bentuk raspberi hierarki, bentuk bipyramid heksagon dipenggal, bentuk bunga, partikel berbentuk panjang dan quasi kiub. Semua partikel hierarki ini mempamerkan sifat-sifat magnet yang unik. Sampel yang disediakan daripada 1mmol kobalt klorida, 2 mmol natrium hidroksida, 5 mmol hidrazin hidrat dan 3.0% (w/v) natrium sulfat dodesil mempunyai campuran partikel berbentuk kubus dan kuasi memanjang. Ia mempunyai koerciviti tertinggi kira-kira 290 Oe. Partikel kobalt emas dwilogam dengan struktur hierarki juga telah disediakan melalui tindak balas penggantian galvanik yang mana kobalt bertindak sebagai templat pengorbanan. Partikel dwilogam dengan struktur hierarki berongga dan beberapa bentuk lain yang

arbitrari telah dihasilkan dengan keadaan sintesis yang berbeza. Secara umumnya, partikel dwilogam luhur/magnetik didapati mempunyai sifat magnet yang dipertingkatkan berbanding partikel kobalt tulen. Peratusan baki kandungan kobalt dalam sampel kobalt/emas telah ditentukan menggunakan spektroskopi serapan atom. Partikel kobalt dalam sampel kobalt/emas disintesis dengan kepekatan  $\text{HAuCl}_4$  yang berbeza pada suhu bilik menunjukkan nilai  $M_s$  yang dipertingkatkan berbanding dengan kobalt tulen. Nilai  $M_s$  untuk semua partikel kobalt selepas penggantian galvanik semuanya lebih tinggi daripada 124 emu/g untuk partikel kobalt tulen. Sampel yang disediakan pada  $100^\circ\text{C}$  dengan 5ml  $\text{HAuCl}_4$  (5mM) dengan bentuk arbitrari mempamerkan koerciviti tertinggi dan dipertingkatkan iaitu 523 Oe.

# **ROLE AND CORRELATION OF SYNTHESIS, SIZE AND MORPHOLOGY TO THE MAGNETIC PROPERTIES OF COBALT AND COBALT/GOLD BIMETALLIC HIERARCHICAL NANOSTRUCTURES**

## **ABSTRACT**

Cobalt is a ferromagnetic material while cobalt-gold bimetallic particles are expected to have modulated magnetic properties. Besides, gold nanostructure is also a good plasmonic material. However, cobalt is susceptible to oxidation in aqueous environment. The oxidised layer can harm the magnetic properties. Therefore, in order to avoid oxidation of cobalt, this work was devoted to the synthesis of cobalt and cobalt-gold bimetallic hierarchical particles using polyol method cum galvanic replacement reaction. A number of synthesis conditions were experimented in order to investigate their impacts on the morphologies of the cobalt particles produced. The parameters studied including reaction time, sodium hydroxide, concentration of cobalt salt, reaction temperature, reducing agent and surfactants. Various morphologies were successfully prepared such as hierarchical microspheres, hierarchical polyhedral shape, hierarchical raspberry like, truncated hexagonal bipyramid, flower-like, elongated and quasi cubic-like particles. All of these hierarchical cobalt particles exhibited their own unique magnetic properties. Sample prepared from 1mmol cobalt chloride, 2 mmol of sodium hydroxide, 5 mmol of hydrazine hydrate and 3.0% (w/v) of sodium dodecyl sulfate has a mixture of quasi cubic and elongated particles. It has the highest coercivity of about 290 Oe. Cobalt-gold bimetallic hierarchical particles were prepared by galvanic replacement reaction where cobalt acted as sacrificial template. Bimetallic particles with hollow hierarchical structure and arbitrary shapes were produced under different synthesis conditions. Generally, these noble/magnetic bimetallic particles were found to have

enhanced magnetic properties compared to the pure cobalt particles. After galvanic replacement, percentages of remaining cobalt contents in the cobalt-gold samples were determined by atomic absorption spectroscopy. Cobalt particles in the cobalt-gold bimetallic samples synthesised with different  $\text{HAuCl}_4$  concentration at room temperature shows enhanced  $M_s$  values compared to the pure cobalt. The coercivity values of the cobalt particles after galvanic replacement are all higher than that of the pure cobalt particles before the replacement reaction. Cobalt/gold bimetallic sample prepared at  $100^\circ\text{C}$  with 5ml  $\text{HAuCl}_4$  (5mM) with arbitrary shape exhibited highest and enhanced coercivity of 523 Oe.

# CHAPTER 1

## INTRODUCTION

### 1.1 Nanomaterials

Nanomaterials are the essential building block to allow development of nanotechnology. According to ISO TS 80004-1:2010, the word “nanomaterials” is referred to the materials with any external dimension in the nanoscale or having internal or surface structure in the nanoscale. Nanoscale according to ISO/TS 27687:2008 is defined as the size range from approximately 1 nm to 100 nm. Nanomaterials usually exhibit different properties and behaviour as compared to bulk materials with similar chemical composition. This is mainly due to the size effect.

Nanomaterials can be classified into two main categories: (i) compact materials and (ii) nanodispersions. The first type includes so-called *nanostructured materials*. Nanostructured materials are materials isotropic in the macroscopic composition and consisting of contacting nanometer-sized units as repeating structural elements. *Nanodispersions* on the other hand include a homogeneous dispersion medium (vacuum, gas, liquid, or solid) and nanosized inclusions dispersed in this medium and isolated from each other (Gubin, 2009). Nanomaterials can be classified into 0 Dimension (0D) like nanoparticles, 1 Dimension (1D) like nanorods or nanowires and 2 Dimension (2D) like nanofilm and nanosheets.

### 1.2 Hierarchical nanostructures

A ‘hierarchical structure’ means a higher dimension of a micro- or nanostructure composed of many, low dimensional, nano-building blocks such as 0

D nanoparticles, 1D nanowires, nanorods, and nanotubes, and 2D nanosheets. The various hierarchical structures can be classified according to the dimensions of nano-building blocks and the consequent hierarchical structures, referring to the dimensions, respectively, of the nano-building blocks and of the assembled hierarchical structures (Lee, 2009). The nomenclature of the hierarchical structures will be discussed in Chapter 2. There are various materials that can be synthesised to yield to the hierarchical structure. Metal particles for instance will show novel properties when made in hierarchical structure and they also possess authentic beauty.

### **1.3 Background study and problem statement**

In the past decades, cobalt magnetic nanomaterials have been successfully synthesised and their size dependent unique properties have been explored. 0D nanoparticles, 1D nanowires and 2D nanoplates of cobalt have been produced. Cobalt hierarchical nanostructures assembled from these lower dimensional nanomaterials have however only attracted attention in the recent years. Reports on successfully synthesised cobalt hierarchical structures include snowflake-like, cauliflower-like and ball-like particles (Liu et al., 2009c), hexagonal microspheres with ultrathin nanoflakes (Yang et al., 2009a), flower-like structures (Zhang et al., 2008a), rice ear-like microstructures (Li et al., 2010), pine-tree-leaf like (Li and Zeng, 2010), chain-like (Wang et al., 2011) and dendritic structures (Sivasubramanian and Sangaranarayanan, 2012). Of all these structures, dendritic structure is the most successfully synthesised hierarchical structure for cobalt.

Since cobalt is a ferromagnetic material, the study on how its magnetic behaviour would be affected by the hierarchical structure is very interesting to be

explored. Understanding this would open up possibilities of the use of cobalt in various industries. Modulating magnetic properties of the cobalt has also been investigated by many researchers. Shape anisotropy is one of the many factors that can modulate the magnetic properties (Cowburn, 2000, Liu et al., 2008). Bimetallic or combination of magnetic/noble metals can induce modulating magnetic properties as reported by Ely and Fromen groups (Ely et al., 2000, Fromen et al., 2002). Noble or gold nanoparticles possess sensitive adsorption in optical wavelength. Combining cobalt and gold has been speculated to produce bimetallic particles with unique properties. In this case, gold is more electronegative than cobalt and the interactions between the two components will influence on the neighbouring atoms leading to novel properties which cannot be observed when the components are in its individual element (Pal et al., 2006). It is obvious that combining cobalt and gold to produce bimetallic particles to modulate the magnetic properties is feasible. There are only very few reports on cobalt-gold bimetallic hierarchical structures in the literatures (Wetz et al., 2007, Lu et al., 2010, Min et al., 2011).

In this study, such structure was synthesised. Various approaches were employed to synthesise hierarchical nanostructures especially by hydrothermal method. This method has been use widely with water often used as solvent. However, cobalt is susceptible to oxidation hence will oxidise in water. Therefore, organic solvent is thought to be a better choice as solvent. In this project, polyol process was used. Polyol process is a simple and versatile non-aqueous route developed by Fievet and coworkers (Fievet et al., 1989b) to synthesise various metal particles. Solvents such as ethylene glycol, diethylene glycol and triethylene glycol are classified as polyol. Compared to aqueous methods, nanoparticles synthesised

from polyol process are protected by surface absorbed polyol molecules, thus minimising the chances of oxidation of the particles. This non aqueous solvent, also further reduced the problem of hydrolysis of fine metal particles as often occurred in the aqueous case (Willard et al., 2004). Besides functioning as solvent, polyol such as ethylene glycol can also act as capping agent in some cases (Ningthoujam et al., 2008, Vinod et al., 2011). Because of this, the formation of anisotropic particles in the polyol are possible. Polyol is also a more environmentally friendly and economical method (Yang et al., 2008, Kim et al., 2009). It does not need an expensive reactor unlike the hydrothermal and chemical vapour deposition (CVD) processes. CVD also requires high temperature and toxic corrosive gases normally employed in the process. Considering all these, polyol process was chosen to synthesise cobalt hierarchical particles in this work.

From the theoretical consideration, metal ions with higher reduction potential can accept electrons from a solid metal with lower reduction potential, that is, more noble metal ions can be reduced into a solid by taking electrons from a less noble metal solid. Therefore, another synthesis route based on this theory or so called galvanic replacement reaction has recently become a key and novel means toward syntheses of diverse nanomaterials of hollow, porous and bimetallic hierarchical nanostructures. The replacement reaction between metal particles (sacrificial template) and noble salt precursor containing a relatively less active metal plays a crucial role in this type of reaction. No additional reducing agents are needed in the reaction. Another added advantage of this method is various types of hierarchical anisotropy materials which can be synthesised even without incorporation of

surfactant. Therefore, this electrochemical process open the door to the preparation of various novel nanomaterials (Moon et al., 2011).

In the past, cobalt hierarchical nanostructures were mostly prepared by hydrothermal or solvothermal process. Very little works are reported using polyol process. Those limited works on producing hierarchical cobalt particles using polyol process are presented in the Table 1.1. From Table 1.1, it can be observed that the polyol process employed addition of nucleating agent (Yang et al., 2010) or external magnetic field is being applied (Dakhlaoui et al., 2008, Zhang et al., 2011a). In this work, no nucleating agent or external field is applied. Ethylene glycol (EG) is chosen as solvent because of its high boiling point (190°C) and it is a polar solvent which can dissolved different ionic compounds, for instance, cobalt chloride hexahydrate which is used in our case.

Table 1.1 Cobalt hierarchical particles synthesised via Polyol process in the past.

Chemical in used /reaction condition	Morphology/ shape	References
Solvent: EG Co(Ac), NaOH, N <sub>2</sub> H <sub>4</sub> <i>External magnetic field of 500 Oe</i>	Fibre (wire-like)	(Dakhlaoui et al., 2008)
Solvent: EG Co(Ac), PVP, <i>Nucleating agent: palladium chloride</i>	Hollow spheres and hemispheres	(Yang et al., 2010)
Solvent: EG CoCl <sub>2</sub> , N <sub>2</sub> H <sub>4</sub> , NaOH <i>External magnetic field of 4000 Oe</i>	Wire -like	(Zhang et al., 2011a)

Meanwhile, works on the synthesis of cobalt/gold bimetallic hierarchical particles by galvanic replacement reaction in the past are listed in the Table 1.2. As can be seen from the Table 1.2, none of the reactions was conducted in polyol solvent. Thus, polyol was chosen as medium for replacement reaction in this work as it can prevent the oxidation of cobalt during the replacement reaction.

Table 1.2 Co/Au hierarchical bimetallic particles produced from galvanic replacement reaction in the past.

Chemical in used	Morphology/ shape	References
Solvent: Dicholobenzene Cobalt and H <sub>Au</sub> Cl <sub>4</sub>	Core-shell particles	(Mandal and Krishnan, 2006)
Solvent: Toulene Cobalt and AuCl(tht) (tetrahydrothiophene)	Hybrid nanorods	(Wetz et al., 2007)
Solvent: Aqueous Cobalt and H <sub>Au</sub> Cl <sub>4</sub>	Yolk-shell spheres	(Lu et al., 2010)
Solvent: Aqueous Cobalt and H <sub>Au</sub> Cl <sub>4</sub>	Microwire with nanoflakes	(Min et al.2011)

Therefore, this work is directed towards synthesis of cobalt and cobalt-gold bimetallic with hierarchical nanostructures with different morphologies using modified polyol process and galvanic replacement reaction (polyol as solvent) respectively. The parameters that we modified in the polyol process include different synthesis conditions (shown in scope of work) and addition of various types of surfactants during the synthesis. It is hoped that new morphologies obtained (with shape anisotropy) can lead to some enhanced or novel properties which are useful and rendered them some potential applications.

#### **1.4 Objectives of work**

1. To synthesise cobalt particles with varying hierarchical structures by polyol method.
2. To investigate the magnetic properties of synthesised cobalt formed with different sizes and morphologies.
3. To produce cobalt/gold hierarchical bimetallic particles by galvanic replacement and characterise their magnetic properties.

#### **1.5 Scope of work**

This thesis is divided into 2 parts. First part is the synthesis of the cobalt particles with different hierarchical nanostructures by polyol process. Cobalt hierarchical nanostructures were synthesised with different synthesis conditions, including: reaction time, sodium hydroxide (NaOH), concentration of cobalt salt:  $\text{CoCl}_2 \cdot 6\text{H}_2\text{O}$ , reaction temperature, reducing agent: (i) Hydrazine hydrate and (ii) Sodium Borohydride, surfactants (i) Polyvinylpyrrolidone K30 (PVPK30), (ii) Cetyl trimethylammonium Bromide (CTAB) and (iii) Sodium dodecyl sulphate (SDS).

Second part was to produce bimetallic cobalt/gold particles with hierarchical nanostructures through galvanic replacement reaction with selected spherical cobalt particles acting as sacrificial template and  $\text{HAuCl}_4$  as the gold salt. Different synthesis conditions have been set such as amount of gold salts ( $\text{HAuCl}_4$ ), effect of temperature and effect of NaOH. All the samples produced were characterised by various tools and their magnetic properties are investigated based on their size and morphology.

## CHAPTER 2

### LITERATURE REVIEW

#### 2.1 Introduction to nanomaterials

A general definition of the *nanomaterials* state that nanomaterials are materials where the sizes of individual building blocks are less than 100 nm, at least in one dimension (Vollath, 2008) This definition is well applicable for many research proposals where nanomaterials have a high priority. Nanomaterials is an area which requires interdisciplinary basic knowledge from physics, chemistry and material science in order to understand the properties and behavior of nanomaterials. Many applications of nanomaterials are related to biology and medicine, therefore the knowledge of these areas are required as well (Vollath, 2008). This can be well understood and visualized from Figure 2.1.

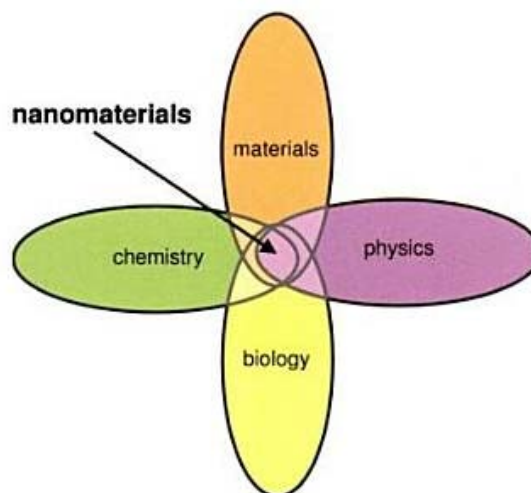


Figure 2.1 Nanomaterials lie at the intersection of materials science, physics, chemistry and biology or medicine (Vollath, 2008).

Nanomaterials could exist in zero dimension (0D), one dimension (1D), two dimension (2D) and three dimension (3D) (Pokropivny and Skorokhod, 2007). Zero

dimensional (0D) materials normally referred to spherical nanoparticles and is “isotropic” nanomaterials. On the other hand, 1D, 2D and 3D nanomaterials are called “anisotropic” nanomaterials. Various anisotropic nanomaterials are reported in the literature. Table 2.1 summarizes some of the anisotropic materials according to their dimensionality.

Table 2.1 Different anisotropic nanomaterials group with different dimensionality (Rotello, 2004b).

<b>Anisotropic materials</b>	<b>Examples</b>
1 dimension (1 D)	Nanorods, nanowires, nanotubes
2 dimension (2 D)	Nanoplates, nanosheets
3 dimension (3 D)	Nanocubes, nanoboxes, nanorice

After the discovery of carbon nanotubes by Iijima (Iijima, 1991), the 1D nanostructured nanomaterial has been considered as a standard example which exhibits unique physical and chemical properties. Numerous works were devoted to the shape-dependent synthesis of diverse nanomaterials. This is partly due to the fact that particle anisotropy offers different physical and chemical properties that are difficult to obtain simply by size-tuning of spherical nanoparticles.

## **2.2 Size and surfaces in nanomaterials**

Nanostructures and nanomaterials possess a large fraction of surface atom per unit volume. This can be seen from Figure 2.2 which presented the percentage of the surface atoms changes with the palladium cluster diameter (Nutzenadel et al., 2000). Such a drastically changed in percentage of the surface atoms when a particle/cluster getting smaller in nano-region can lead to great changes in physical and chemical

properties of the nanomaterials (Cao, 2004). These properties include optical (Ploschner et al., 2012), magnetic (Watari and Ohnishi, 1998), melting points (Nanda, 2009), oxidation temperature (Montiel et al., 2011) to name but a few.

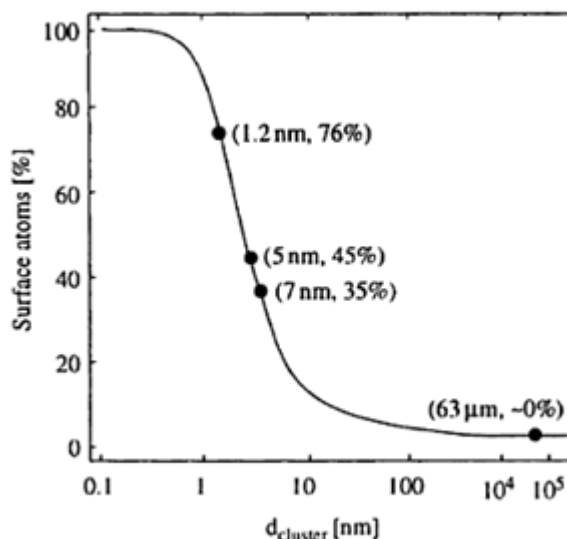


Figure 2.2 The percentage of surface atoms changes with the palladium cluster diameter (Nutzenadel et al., 2000).

For instance, the noble metal platinum is a non-magnetic element in the bulk. However, as reported by Watari and Ohnishi (1998), when the size of Pt clusters decreased and consisting of  $13 \pm 2$  atoms, it exhibit extraordinary magnetic polarisation with up to 8 unpaired electrons on a cluster, corresponding to a magnetic moment of  $0.65 \mu_B$  per atom. In another report (Montiel et al., 2011), bulk cobalt start to oxidise in air at roughly  $350^\circ\text{C}$ . However, nanoparticles with size range of 20 to 57 nm start to oxidise in air at the temperature as low as  $150^\circ\text{C}$ . This shows that size and surface area play a crucial role in determine the properties of nanomaterials.

The surface energy is related to surface area and increases as the overall surface area increased when size of particles getting smaller (Cao, 2004). Therefore, nanostructured materials normally possess a large surface energy. For the thermodynamic consideration, the surface energy per mol of material is the essential

quantity (Vollath, 2008). The equation derived for surface energy per mol ( $U_{\text{surface}}$ ) is shown in equation 2.1 (Vollath, 2008).

$$U_{\text{surface}} = \frac{6M\gamma}{\rho D} \quad (2.1)$$

Where M is the molar weight,  $\gamma$  is the specific surface energy,  $\rho$  is the density of material, D is the particle diameter. As can be seen from equation 2.1, the surface energy per mol increases with  $\frac{1}{D}$ . In the other words, when the particles getting smaller, the increasing surface energy is significance especially in the nano region. Nanomaterials with high surface energy are not stable. Therefore, the system tend to reduce the overall surface energy in order to reach a stable stage.

Generally, reduction of the overall surface energy can be achieved through (i) combining the individual nanomaterials together in order to form a larger structures and (ii) agglomeration/ aggregation of individual nanomaterials without altering the individual nanomaterials (Cao, 2004). There are two ways of combining individual nanomaterials to form larger structures which are *sintering* and *Ostwald ripening*. In the sintering process, the individual nanomaterials are packed in such a way that there is no gap among solid nanomaterials. Whereas in Ostwald ripening process, two individual nanomaterials becomes single one. Smaller one will feed the larger one until it was totally disappeared. In agglomerate/aggregation, many nanomaterials are associated with one another through chemical bonds and physical attraction forces. The smaller the individual nanomaterials are, the stronger they are formed and more difficult to separate.

Since nanomaterials possess high surface energy are not stable, minimisation of the surface energy has been reported as an important factor or driving force for the

self assembly of nanomaterials (Zhang et al., 2011b, Wang et al., 2010c, Song and Colfen, 2010, Zhang et al., 2005b, Wang and Feng, 2003). Wang and Feng (2003) have investigated the formation of the polyhedral shape of CeO<sub>2</sub> Nanoparticles. During the aggregation process, the particles tend to share common faces in order to maximise the packing density. This is a general principle in forming a self-assembled nanostructure. When two particles are in contact, they tend to rotate themselves in order to achieve a position with minimal energy and least lattice mismatch. Therefore, a *coherent interface* is formed as presented in Figure 2.3.

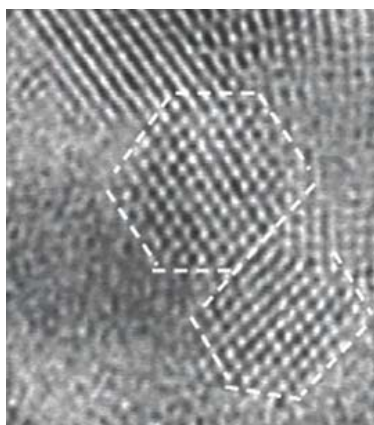


Figure 2.3. Two particles with face-to-face contact and coherent interfacial matching (Wang and Feng, 2003).

A very interesting and excellent work related to surfaces of nanoparticles has been reported by Vollath (2008). In this work, the mechanism of aggregation of two single gold nanoparticles has been observed through high resolution transmission electron microscopy from the very beginning until the aggregate formed. From the observation, when the two nanoparticles are in contact, they rotate until their orientation is equal (with parallel lattice fringes). This is similar to the report of Wang and Feng (2003) where a coherent interface with minimal energy was achieved. After this, the aggregation begins as the larger particles engulf the smaller one. The energy required for this process occurred actually provided by the reduction of the surface area.

### 2.3 Hierarchical nanostructures

Currently there is a new kind of nanostructured materials that has attract a lot of attention – hierarchical nanostructures. A ‘hierarchical structure’ means the higher dimension of a micro- or nanostructure composed of many, low dimensional, nano-building blocks. Generally, various hierarchical structures are classified according to the dimensions of the nano-building blocks and the consequent hierarchical structures (Lee, 2009). For instance, “0-3 hollow” means 0D nanoparticles are assembled into a 3D hollow spherical shape. This type of 0-3 hierarchical particles normally has a smooth surface (Lee, 2009). The nomenclature of various hierarchical structures is shown in Figure 2.4.

Self-assembly of nanomaterials into hierarchical structures largely depends on their shape, surface properties, charge, magnetic dipole forces and so on. Hence, from the same building blocks, organisations having different properties can be created depending on the dimensionality as well as the nature of interaction between the nano-building blocks (Sajanlal et al., 2011).

These hierarchical nanostructures bring novel properties which are entirely different from the properties of individual and bulk counterpart (Pileni, 2001). For example, hierarchical magnetite ( $\text{Fe}_3\text{O}_4$ ) microspheres nanostructures which were self-assembled from 45nm nanoparticles holds an unique microwave electromagnetic properties compared to the conventional magnetite microspheres (Zhao et al., 2010a). The hierarchical magnetite microspheres exhibited a microwave magnetic loss peak at high frequency region which is never observed in the conventional microspheres.

The authors had confirmed the high frequency magnetic loss peak is attributed to the hierarchical structure through a simulation using Matlab software.

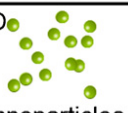
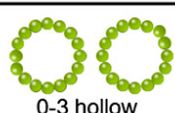
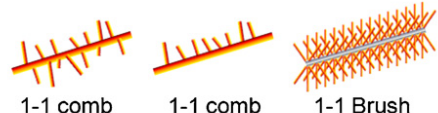
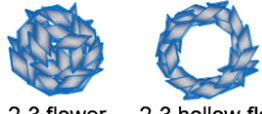
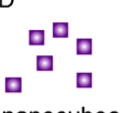
Nano Building Blocks	Hierarchical nanostructures
0-D  nanoparticles	 0-3 hollow
1-D  nanowires, nanorods	 1-1 comb    1-1 comb    1-1 Brush
	 1-2 dendrite
	 1-3 urchin    1-3 thread    1-3 hollow urchin
2-D  nanosheets	 2-3 flower    2-3 hollow flower
3-D  nanocubes	 3-3 hollow

Figure 2.4 Nomenclature of hierarchical structures according to the dimensions of the nano-building blocks (the former number) and of the consequent hierarchical structures (the latter number)(Lee, 2009).

The novel or unique properties of the hierarchical materials is attributed to the restricted motion of electrons, holes, phonons and plasmons which is related to the *physical shape* of the nanomaterials (Sajanlal et al., 2011). For instance, a spherical shape particle, the electrons are confined to the same extent in all the three dimensions. Therefore, the properties will be roughly the same regardless of directions. Tuning the properties of these particles will be difficult if compared to other materials with anisotropic shape. In addition to the novel properties, such

hierarchical structures also possess both authentic beauty and novel functionalities which can further link with other bio-molecules (Li and Zeng, 2010).

#### **2.4 Synthesis approaches of various type of nanomaterials/nanostructures**

Many techniques, including both top-down, intermediate and bottom-up approaches, have been developed and applied for the synthesis of nanomaterials. The preparation method of nanomaterials represents one of the most important challenges that will determine the particle size, shape, structure and surface chemistry of the particles (Tartaj et al., 2003). Consequently, properties of the nanomaterials will be affected as well. Generally, the most favourable synthesis approaches of nanomaterials are chemical (bottom up) and physical (top down) approach. For the synthesis of nanomaterials, chemical approach is proven to be the more efficient route. Some of the typical chemical methods such as hydrothermal or solvothermal process, polyol process and galvanic replacement reaction have been summarized and discussed in this session. Figure 2.5 shows the general approaches to synthesise bulk nanostructured solids.

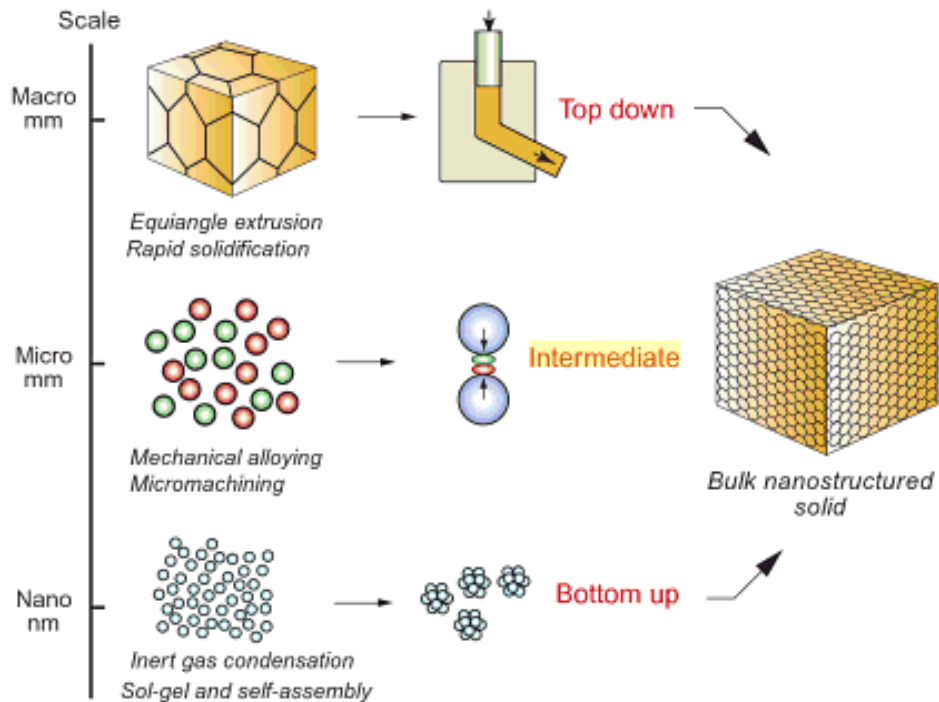


Figure 2.5 Illustration showing the top down, intermediate and bottom up approaches to make bulk nanostructured solids (Ashby et al., 2009).

#### 2.4.1 Hydrothermal or Solvothermal process

Hydrothermal process is a very popular process in the synthesis of nanomaterials. The term “hydrothermal” was originally first used by a British Geologist, Sir Roderick Murchison (1792–1871), to describe the action of water at elevated temperature and pressure in bringing about changes in the earth’s crust leading to the formation of various rocks and minerals (Byrappa and Yoshimura, 2001). Solvothermal method is similar to the hydrothermal method except that organic solvents are used instead of water. This method can effectively prevent the products from oxidizing and has been used to synthesise a variety of non-oxides. Some of the hierarchical structure nanomaterials produced by this process will be discussed in the following section.

Hydrothermal synthesis refers to the synthesis by chemical reactions of substances in a sealed heated solution above ambient temperature and pressure. The autoclaves used in hydrothermal synthesis are usually thick-walled steel cylinders completely sealed which can withstand high temperatures and pressures for prolonged period of time. Furthermore, the autoclave material must be inert with respect to the solvent. The closure is the most important element of the autoclave. Under the hydrothermal conditions, various nanomaterials and materials with hierarchical nanostructures were synthesised. For example, a novel nickel nanobelts were generated by reducing nickel tartrate complex in alkaline solution with the surfactant (SDBS) at temperature 110°C. This hydrothermal process was performed for 24 hours. The nanobelts obtained consisted of typical width of 500-1000nm. A thickness of about 15 nm and a length of up to 50  $\mu\text{m}$  was measured. Surfactant SDBS has a remarkable effect on the formation of Ni nanobelt in this hydrothermal process (Liu et al., 2003).

In another work, nickel hierarchical nanostructures with urchin and sisal-like morphologies also had been successfully prepared employing hydrothermal process (Wang et al., 2007b). The electron micrographs of these unique morphologies are shown in the Figure 2.6. The addition of surfactant (CTAB), hydrazine hydrate and the present of glycine play a crucial role in influencing the morphologies of the final products. The magnetic properties measured for these nickel hierarchical nanostructures were enhanced compared to their bulk counterpart.

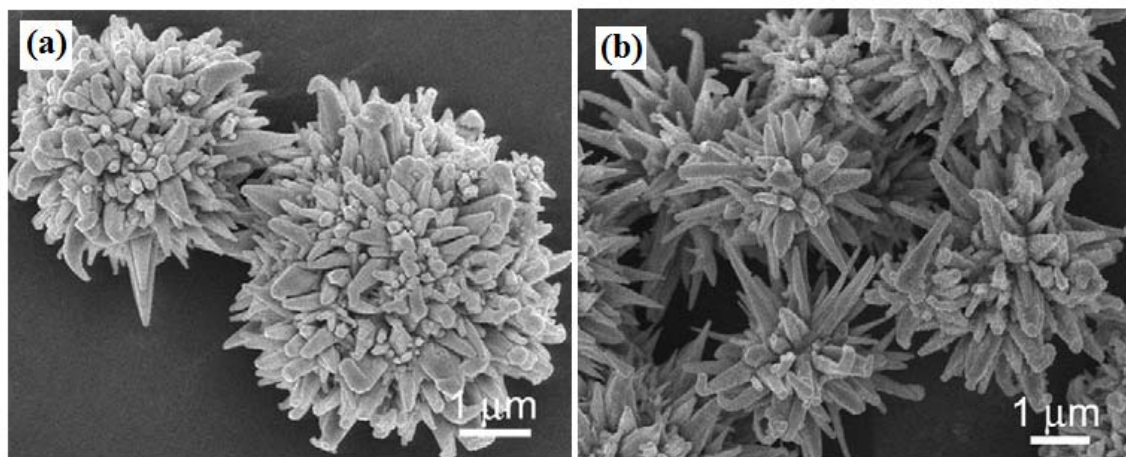


Figure 2.6 SEM images of nickel hierarchical nanostructures with (a) urchin like and (b) sisal like morphologies (Wang et al., 2007b).

In another work by Jing and Wu (Jing and Wu, 2004), monodisperse rhombohedral  $\alpha$ -Fe<sub>2</sub>O<sub>3</sub> particles have also been synthesised by hydrothermal method with the incorporation of four surfactants, i.e. SDS, DBS, CTAB and HPC, using FeC<sub>2</sub>O<sub>4</sub> and NaOH as starting precursors. All the samples after modified with surfactant transformed from rod-like to rhombohedral shape, and the particle size of each sample has clearly changed. Particle shape induced by the surfactants resulted in shape anisotropy, and furthermore coercivity of the samples after modification were enhanced (Jing and Wu, 2004). Uniform hematite nanocubes with an average size of 15 nm have been also prepared using this method. It was revealed that the molar ratio of iron chloride to sodium oleate and hydrothermal temperature had a crucial influence on the morphology of hematite nanoparticles produced in the synthesis (Wang et al., 2007a).

Hierarchical Co nanoflowers composed of nanorods were fabricated through a solvothermal process. 1,2-propanediol was used as solvent instead of water (Liu et al., 2009a). Well-defined nanoflowers of about 500 nm having petals with lengths of

about 500 nm and diameters of 50 nm were obtained (Figure 2.7). In this case, hexadecylamine, the structure-directing agent plays an important role in regulating the growth of the flowery nanostructure through its strong adsorption onto the cobalt nanocrystals, leading to a hierarchical growth mode. Cobalt nanofibres with pine-tree-leaf hierarchical superstructures also have been synthesised through this solvothermal process in which diethylene glycol was used as solvent. The solvothermal temperature was kept at 200°C for all the reactions in preparing the cobalt fibres (Li and Zeng, 2010).

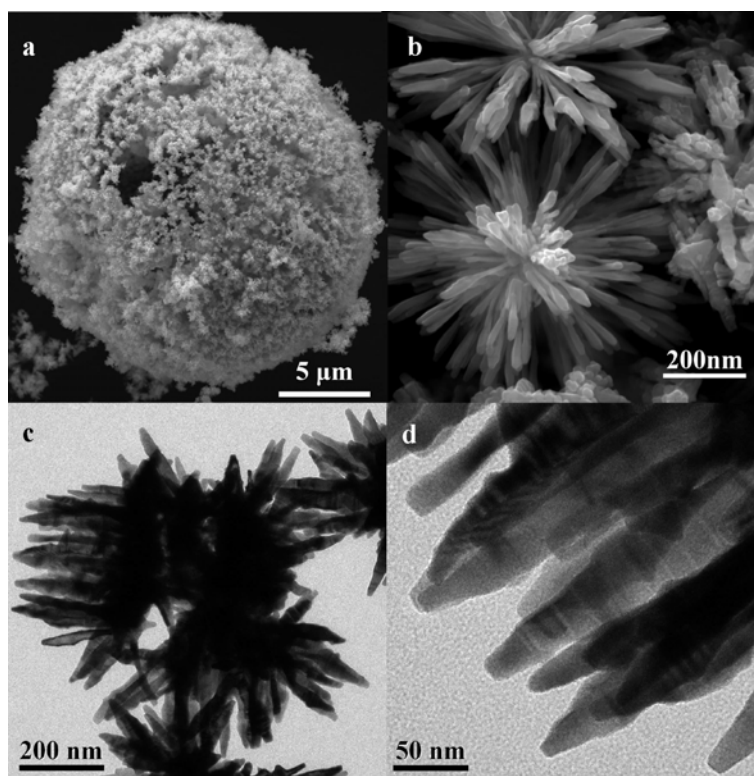


Figure 2.7 (a,b) SEM and (c,d) TEM images of the Co nanoflowers (Liu et al., 2009a).

Besides the magnetic materials with nanostructures, diversity of other materials also have been successfully prepared through this method. Zhu and co-workers (Zhu et al., 2009) have demonstrated that PbTe with various hierarchical

nanostructures, including hopper cubes, flower-like structures, and dendritic structures were synthesised via this simple hydrothermal process (Figure 2.8). Different synthesis parameters such as reaction time, temperature, concentration of sodium hydroxide, and surfactants, were systematically investigated. Sodium hydroxide was proposed to play a crucial role in the formation process. The authors suggested that the formation of hierarchical PbTe nanostructures is due to the deviation of the formation conditions from the thermodynamic equilibrium. Near the equilibrium conditions, specific polyhedral forms are created through a kinetic controlled reaction. Under far equilibrium conditions, the instability of the growing fronts of crystals leads to the formation of dendritic morphology (due to increased contribution of mass or heat diffusion). Hopper cubic structures are formed due to the non-uniformity of the solute distribution over the crystal faces.

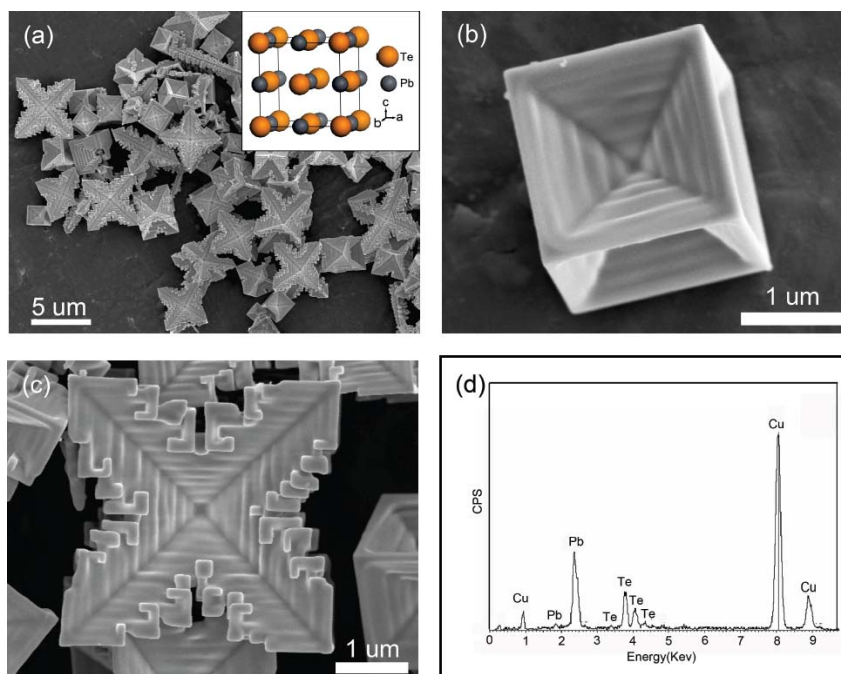


Figure 2.8 (a) Typical SEM image of PbTe hierarchical nanostructures. Inset: unit cell of PbTe. (b) Magnified image of a hopper cubic crystal. (c) Magnified image of a flower-like crystal. (d) EDX spectrum of PbTe superstructures (Zhu et. al., 2009)

Recently, a very interesting ZnO hierarchical nanostructure was synthesised via this hydrothermal route (Figure 2.9). The hierarchical nanostructure has morphology similar to the natural pine tree forest. Thus, the artificial hierarchical nanostructure was named “nanoforest”. The “nanoforest” grew with high density, long branched “treelike” with multi-generation hierarchical ZnO nanowires which can significantly increase the dye-sensitized solar cells (DSSC) power conversion efficiency. (Ko et al., 2011).

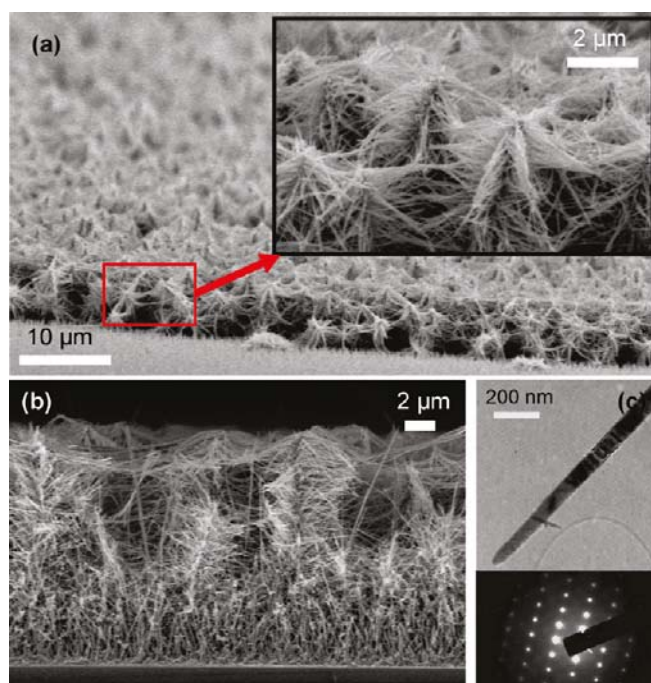


Figure 2.9 SEM pictures of ZnO NW nanoforest: (a) tilted view, (b) crosssection view, (c) TEM picture and selected area electron diffraction pattern of a ZnO NW (Ko et al., 2011).

Hydrothermal or solvothermal are very popular methods among materials scientists or researchers. A variety of materials have been synthesised through this method. Table 2.2 below shows the various materials with hierarchical nanostructures synthesised via this method.

Table 2.2 Various materials with hierarchical structure synthesised via hydro/solvothermal in the recent years.

No.	Materials	Morphology	References
1	Bi <sub>2</sub> WO <sub>6</sub>	Hierarchical microspheres (composed of 2D sheets)	(Li et al., 2007)
2	ZnO	Hierarchical Brush like ( composed of nanorods)	(Zhang et al., 2009b)
3	Ni	Hollow Microspheres (composed of nanoparticles)	(Wang et al., 2006)
4	CdS	Hierarchical dendrites	(Qingqing et al., 2006)
5	CeO <sub>2</sub>	Hierarchical flower like	(Yu et al., 2008)
6	Fe <sub>2</sub> O <sub>3</sub>	Hollow Urchin like	(Du and Cao, 2008)
7	CuO	hierarchical butterfly-like architectures	(Zhang et al., 2009a)
8	ZnO	Micropsheres (composed of nanosheets)	(Lu et al., 2011)

The disadvantages of hydrothermal method include the need of expensive autoclaves. Besides, in most of the cases, steel-corroding solutions are used in hydrothermal experiments. In order to prevent corrosion of the internal cavity of the autoclave, protective inserts are generally used. Inserts may be made of carbon-free iron, copper, silver, gold, platinum, titanium or Teflon, depending on the temperature and solution used. Therefore, extra cost was needed. Moreover, high pressure and temperature generated during the reaction also cause a safety issue. The impossibility of observing the reaction process and longer reaction time needed are also the drawbacks of this approach.

#### 2.4.2 Polyol process

Polyol process is a simple and versatile route developed by Fievet and coworkers (Fievet et al., 1989a) to make colloidal particles of various shapes and sizes. Polyols are compounds with “multiple” hydroxyl functional groups available for organic reactions. Therefore, alcohol contains two hydroxyl groups and above

was categorized as polyol. The examples for polyol are ethylene glycol, triethylene glycol, tetraethylene glycol and so forth. Currently, this method has been modified and developed by numerous researchers. The modifications including more additives, for instance surfactant, nucleating agent or assisted by extra devices such as microwaves device. In the polyol process, the liquid polyol acts as the solvent of the metallic precursor, the reducing agent and in some cases as a complexing agent for the metallic cations (ligand binds to metal ions and form complex). One of the advantages of the polyol process is that the pick up of atmospheric oxygen during the reaction is restricted inherently. Generally, in order to prevent oxidation, inert gases like nitrogen and hydrogen or a mixture of these gases is continuously bubbled through the reaction vessel. However, in this method, if hydrazine is used as reducing agent, hydrogen and nitrogen gases are evolved during the reduction of the hydrazine complex, which in turn help the formation of oxide free product. As a result, there is no need for any external blanketing. Therefore, there is no additional costly inert environment needed in this process as the particles can be naturally protected from oxidation by the organic solvent. Apart from this, temperature dependent reducing power and relatively high boiling points also make polyols suitable solvents for producing anisotropic materials.

Diverse nanostructured materials with different sizes and morphologies have been synthesised through polyol process with the assistance of surfactants. Generally, polyvinylpyrrolidone (PVP) is the common surfactant used in the polyol process in order to prevent agglomeration of nanoparticles. Various types of nanoparticles with different size range have been synthesised using this surfactant, such as cobalt (Kalyan Kamal et al., 2009), nickel (Couto et al., 2007), CoPt (An et al., 2008),

CoSb<sub>3</sub> (Yang et al., 2008) and Fe<sub>3</sub>O<sub>4</sub> (Liu et al., 2007a). Besides controlling the particle size and agglomeration, PVP is also used as a shape modifier in the polyol process. Many nano- or micro- size particles with well defined morphology and hierarchical nanostructures have been successfully prepared. A new form of Cu<sub>2</sub>O, disk-like structure with 60 nm in thickness and 2 μm in diameter, has been successfully synthesised in bulk quantities by polyol process in the presence of PVP (Chen et al., 2005c). Without incorporation of PVP, large disk-like shape was produced. This indicates that PVP not only control the growth process but also preventing Cu<sub>2</sub>O nanodisks from increasing in size. In another work by Wang and co-workers (Wang et al., 2008b), chain-like nickel structures assembled with submicrometer-sized hollow spheres has been also successfully prepared with the assistance of PVP. These hierarchical hollow microspheres were found to form through the assembly of small-sized nickel nanoparticles where PVP play a crucial role in the formation process (Figure 2.10).

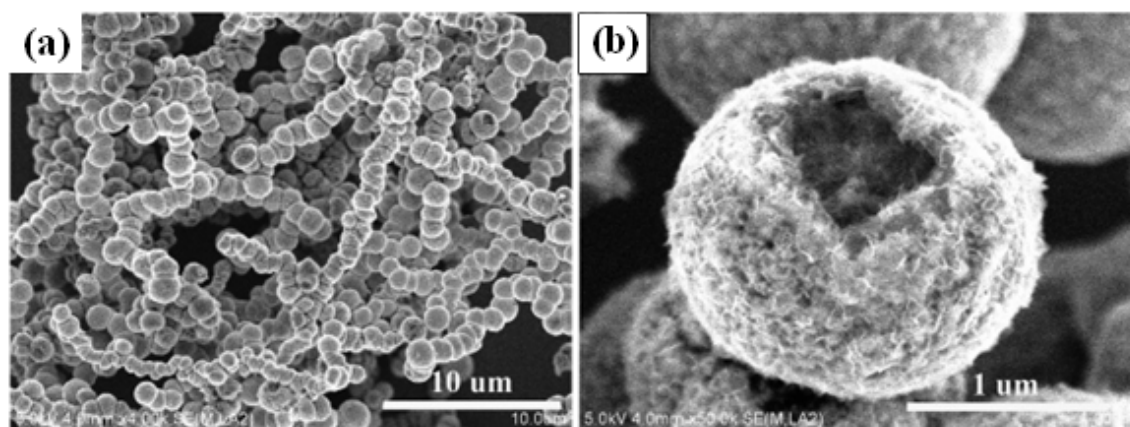


Figure 2.10 (a) SEM image of the as-synthesised Ni microspheres chain network (b) magnified image of single hollow microsphere with hierarchical structure (Wang et al., 2008b).

Beside incorporation of surfactant, Xu's group (Xu et al., 2008b) have modified the polyol process with the aid of microwave source in the reaction